Hindawi
Advances in Condensed Matter Physics
Volume 2017, Article ID 9635219, 12 pages
https://doi.org/10.1155/2017/9635219

Research Article

Development of a Voltage Compensation Type Active SFCL and Its Application for Transient Performance Enhancement of a PMSG-Based Wind Turbine System

Lei Chen,[1] Hongkun Chen,[1] Jun Yang,[1] and Huiwen He[2]

[1]*School of Electrical Engineering, Wuhan University, Wuhan 430072, China*
[2]*State Key Laboratory of Power Grid Environmental Protection, China Electric Power Research Institute, Wuhan 430074, China*

Correspondence should be addressed to Lei Chen; chen_lei@whu.edu.cn

Received 7 July 2017; Accepted 10 October 2017; Published 3 December 2017

Academic Editor: Tao Wang

Considering the rapid development of high temperature superconducting (HTS) materials, superconducting power applications have attracted more and more attention in the power industry, particularly for electrical systems including renewable energy. This paper conducts experimental tests on a voltage compensation type active superconducting fault current limiter (SFCL) prototype and explores the SFCL's application in a permanent-magnet synchronous generator- (PMSG-) based wind turbine system. The SFCL prototype is composed of a three-phase air-core superconducting transformer and a voltage source converter (VSC) integrated with supercapacitor energy storage. According to the commissioning test and the current-limiting test, the SFCL prototype can automatically suppress the fault current and offer a highly controlled compensation voltage in series with the 132 V electrical test system. To expand the application of the active SFCL in a 10 kW class PMSG-based wind turbine system, digital simulations under different fault cases are performed in MATLAB/Simulink. From the demonstrated simulation results, using the active SFCL can help to maintain the power balance, mitigate the voltage-current fluctuation, and improve the wind energy efficiency. The active SFCL can be regarded as a feasible solution to assist the PMSG-based wind turbine system to achieve low-voltage ride-through (LVRT) operation.

1. Introduction

Considering the rapid development of high temperature superconducting (HTS) materials, superconducting power applications have attracted more and more attention in the power industry, particularly for electrical systems with renewable energy [1–6]. Superconducting fault current limiter (SFCL), superconducting magnetic energy storage (SMES), superconducting transformer, and superconducting power cable have obtained lots of successful engineering projects around the world.

In a sense, SFCL may be conducted as a very major application of HTS materials to handle the power transient issues caused by short-circuit faults. When different kinds of SFCLs are used in traditional electrical systems with fossil fuel power plants, there are many candidate locations for installing the SFCLs, such as the large-scale generator terminal, critical transmission line, and key bus-bar. From the existing simulation and experimental results of theoretical models and test prototypes, the expected functions of each type of SFCL are to suppress the fault current without time delay, compensate the voltage sag within an acceptable level, and improve the power system transient stability through the coordination with relay protection [7–10].

Regarding the application of one or more SFCLs in a renewable energy generation system, some basic works have been performed, and a brief literature review is stated as follows. In [11–16], SFCLs such as resistive type and bridge type are used to enhance the operational stability of a wind power plant, and the application feasibility of the SFCLs can be preliminarily confirmed. In [17–19], theoretical and simulation studies are performed to explore the performance of the resistive SFCL used in a microgrid system, which is composed of multiple distributed renewable energy sources.

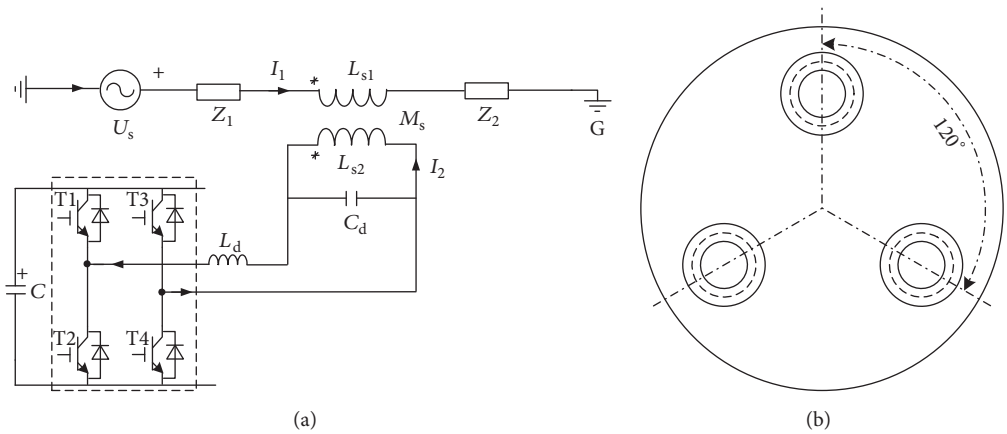

Figure 1: (a) Schematic diagram of the voltage compensation type active SFCL (single-phase connection). (b) Layout diagram of the three individual single-phase superconducting transformers.

As the microgrid is generally connected to the main network via the point of common coupling (PCC) for achieving an economic and reliable power exchange, the SFCL should be located in the direct path of current flowing from the distributed sources and the main network [17, 18]. In addition, employing the resistive SFCL can help to guarantee the service reliability of the microgrid under fault conditions [19], and the technological advantages of the renewable energy sources can be sufficiently highlighted. In [20], the coordinated control of a modified flux-coupling-type SFCL and a SMES unit is proposed for the microgrid. From the demonstrated results, the coordinated control can effectively assist the microgrid to realize a smooth transfer between its grid-connected and islanded modes.

In light of the aforementioned research background, some useful results can be obtained, and more in-depth studies may be done to promote the application of a SFCL in the renewable energy system from multiple aspects. For wind power, lots of studies are focused on doubly fed induction generator- (DFIG-) based wind turbine systems [21, 22]. However, few works are related to the application of a SFCL in a permanent-magnet synchronous generator- (PMSG-) based wind turbine system.

In this paper, our research group is devoted to investigating a voltage compensation type active SFCL prototype and its application for transient performance enhancement of a PMSG-based wind turbine system. The active SFCL is based on power electronic equipment, modern control approach, energy storage technology, and HTS materials. With respect to the active SFCL's theoretical modeling, control strategy, and influence on relay protection as well as power system transient stability, previous studies can be found in [23–26]. On the whole, the active SFCL enables offering higher controllability and flexibility than a common resistive- or inductive-type SFCL. The resistive SFCL cannot easily adjust its current-limiting ability once the working resistance is determined, and the inductive SFCL may not evacuate the surplus active power during the grid fault; however, the active SFCL has the potential capabilities of controlling the current-limiting impedance, smoothing the power fluctuation, and enhancing the power system stability more comprehensively. Additionally, it is expected that using the active SFCL in a PMSG-based wind turbine system can bring more positive effects, including the improvement of its robustness against symmetrical and asymmetrical faults, the reinforcement of its security during an operation of fault ride through, and the stabilization of its parameter indexes of current, voltage, and power.

The organization manner of this paper is stated as follows. Section 2 presents the structural principle of the active SFCL. Section 3 states the configuration description of the active SFCL prototype. In Section 4, the experimental tests of the SFCL prototype are carried out, and the results are analyzed. Section 5 is devoted to exploring the application of the active SFCL in a 10 kW PMSG-based wind turbine system. In Section 6, conclusions are summarized and follow-up works are prospected.

2. Structure and Principle of the Active SFCL

Figure 1(a) indicates the electrical structure of the voltage compensation type active SFCL (single-phase connection) [27]. The active SFCL is mainly composed of three parts, which are, respectively, the air-core superconducting transformer, the voltage-type pulse-width-modulation (PWM) converter with an energy storage unit, and the LC filter. The working philosophy of the active SFCL is to control the current (I_2) flowing in the secondary winding of the air-core transformer by the PWM converter. Based on a mathematical derivation in [28], the active SFCL's equivalent impedance Z_{SFCL} can be expressed as

$$Z_{\mathrm{SFCL}} = j\omega L_{s1} - \frac{j\omega M_s \dot{I}_2 \left(Z_1 + j\omega L_{s1}\right)}{\left(\dot{U}_s + j\omega M_s \dot{I}_2\right)}. \tag{1}$$

In normal condition, adjust I_2 to obtain $Z_{\mathrm{SFCL}} = 0$, and the active SFCL will not affect the main circuit. When a short-circuit fault occurs, the amplitude value and phase angle of

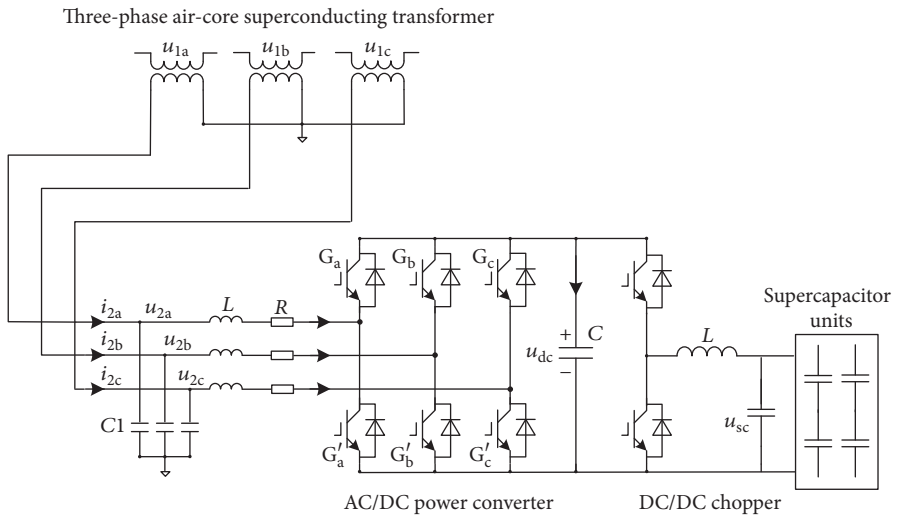

Figure 2: Electrical structure of the active SFCL prototype used in a real three-phase power system.

(a) (b)

Figure 3: (a) Physical diagram of the three-phase air-core superconducting transformer. (b) Physical diagram of the Dewar.

the current I_2 will be regulated, and three current-limiting modes can be basically achieved:

(1) Making I_2 remain the original status, $Z_{\text{SFCL-1}} = Z_2(j\omega L_{s1})/(Z_1 + Z_2 + j\omega L_{s1})$.

(2) Controlling $I_2 = 0$, $Z_{\text{SFCL-2}} = j\omega L_{s1}$.

(3) Regulating the phase angle of I_2 to make the angle difference between $\dot{U}_s$ and $j\omega M_s \dot{I}_2$ be 180°; $Z_{\text{SFCL-3}} = cZ_1/(1 - c) + j\omega L_{s1}/(1 - c)$ is obtained, where the variable c is defined by $j\omega M_s \dot{I}_2 = -c\dot{U}_s$.

When the active SFCL is applied in a three-phase power grid, it is crucial to mitigate and even avoid the magnetic flux disturbances in the three-phase air-core superconducting transformer [29, 30]. For this reason, three individual single-phase air-core superconducting transformers can be properly adopted, and Figure 1(b) shows the layout diagram. In a simplified way, the three transformers are located in the same horizontal plane, and their locations will form an equilateral triangle.

When the PMW converter conducts the control operation, a certain energy exchange will be induced between the main network and the energy storage unit. For the three modes, the energy storage unit should have a rapid response ability, and also different energy requirements will be caused. From [24], the energy exchange for mode 2 is the smallest, and when mode 3 is used to achieve the best current-limiting performance, the energy exchange is the highest. Thus, the capacity design of the energy storage unit should comprehensively consider the three modes.

In theory, the active SFCL has the following technical merits: (1) high controllability due to the PWM converter, (2) great applicability for different voltage grades owing to the adjustment of the transformer, and (3) excellent linearity of Z_{SFCL} thanks to avoiding the magnetic saturation in the air-core.

3. Configuration Description of the Active SFCL Prototype

Figure 2 indicates the electrical structure of the active SFCL prototype used in a three-phase power system, and details of the components are presented as follows.

3.1. Air-Core Superconducting Transformer. Figure 3(a) shows the physical diagram of the three-phase air-core

Table 1: Specifications of a single-phase superconducting transformer.

HTS tape parameters		Transformer parameters	
HTS tape	BSCCO	Structure type	Solenoid
Tape width	4.3 mm	Maximal terminal voltage	800 V
Tape thickness	0.3 mm	Critical current	40 A
Critical current	100 A	Primary/secondary inductance	9.7 mH/32.3 mH
Bending stress	<50 mm	Inner/outer diameter	88 mm/154 mm
Tensile stress	>100 Mpa	Coupling factor	0.83

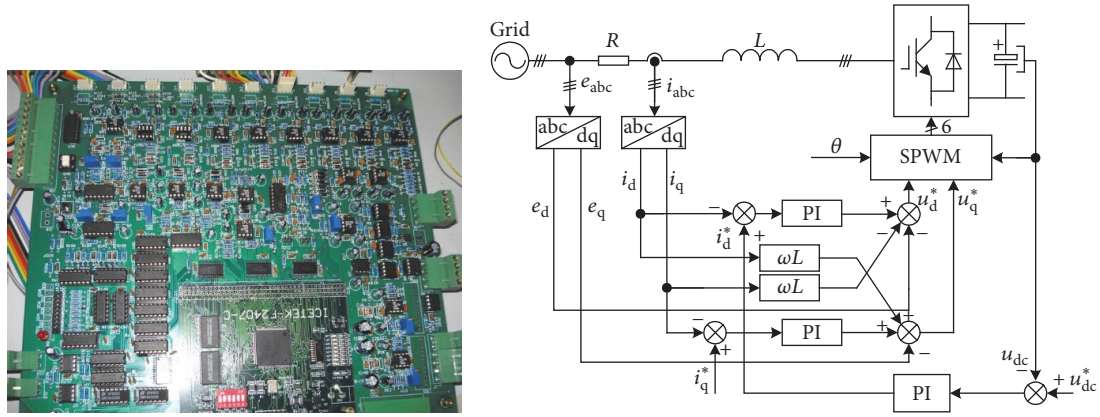

(a) (b)

Figure 4: (a) Control panel based on the digital signal processor (DSP) TMS320LF2407A. (b) Control block diagram of the AC/DC power converter.

Table 2: Specifications of the AC/DC power converter.

Parameters of the AC/DC power converter	
Nominal voltage at AC side	152 V
Nominal frequency at AC side	50 Hz
Nominal capacity	10 kW
Nominal voltage at DC side	400 V
DC capacitance	9400 uF
PWM switching frequency	4.2 kHz

superconducting transformer, whose specifications are denoted in Table 1. Note that the phase-to-phase flux disturbance is avoided, and the coupling factor of the superconducting transformer is about 0.83. Figure 3(b) shows the Dewar which is used to place the superconducting transformer and fill the liquid nitrogen. The inner diameter and height of the Dewar are 500 mm and 530 mm, respectively.

3.2. AC/DC Power Converter. The basic function of the AC/DC power converter is to control the injected currents (i_{2a}, i_{2b}, i_{2c}) in the secondary windings of the three-phase air-core superconducting transformer, and Table 2 shows the main parameters of the AC/DC power converter.

As the core part of the AC/DC power converter, Figure 4(a) shows the control panel which is based on the digital signal processor (DSP) TMS320LF2407 A. By taking advantage of full digitalization information, the control panel can efficiently carry out the double-loop control of the DC voltage (u_{dc}) and the injected AC currents (i_{2a}, i_{2b}, i_{2c}). Figure 4(b) shows the control block diagram of the AC/DC power converter.

3.3. DC Chopper and Supercapacitor Units. For the introduction of the DC chopper circuit, it will serve as a DC to DC converter whose main function is to create an adjustable DC voltage from a fixed DC voltage source through the use of semiconductors. The supercapacitor units will be conducted as the energy storage equipment which is connected to the DC chopper circuit. Since the supercapacitor units are used to act as the DC voltage source and provide the energy support during the dynamic control process, their overall capacity should have a sufficient margin to satisfy the three modes of the active SFCL. Hence, the supercapacitor units will include 80 individual capacitors with the total storage capacity of 300 kJ. The specifications of the DC chopper and the supercapacitor units are indicated in Table 3.

4. Experimental Tests of the Active SFCL Prototype

As shown in Figure 5, it denotes the physical diagram of the active SFCL prototype. In order to assess the performance of the active SFCL prototype, two different kinds of experimental tests have been carried out, and they are the commissioning test and the current-limiting test, respectively.

Table 3: Specifications of the DC chopper and the supercapacitor units.

Parameters of the DC chopper		Parameters of the supercapacitor units	
Nominal current	50 A	Capacitance value	15 F
Output inductance	1 mH	Energy storage capacity	300 kJ
Voltage ratio	200 V/400 V	Nominal voltage	200 V
Switching frequency	10 kHz	Internal resistance	0.16 Ω

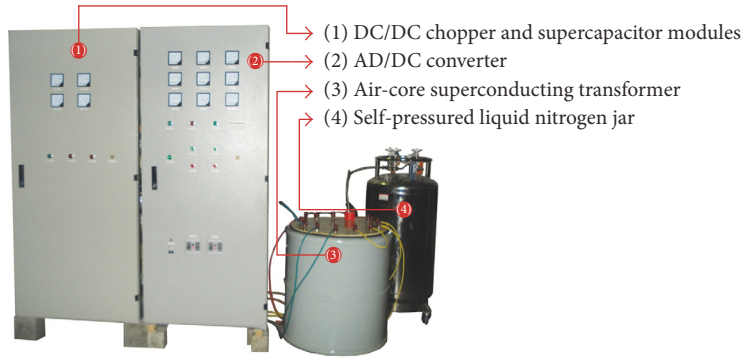

Figure 5: Physical diagram of the active SFCL prototype.

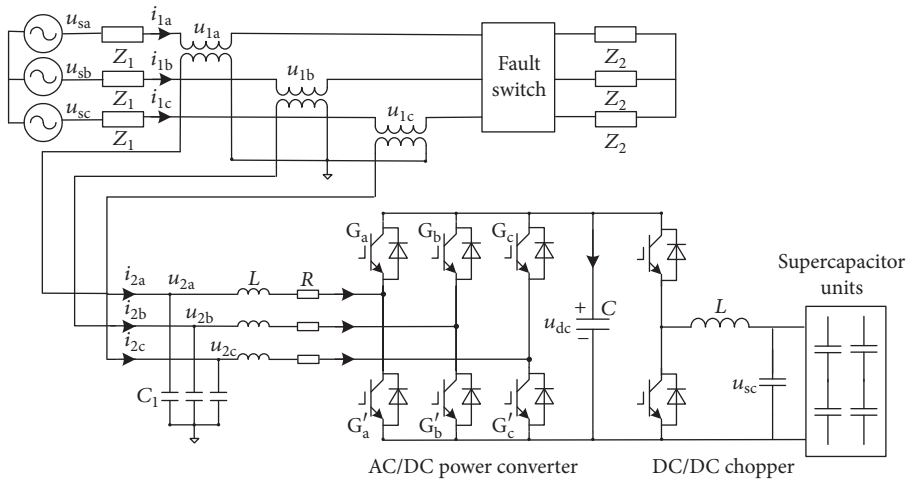

Figure 6: Demonstration of the experimental circuit for testing the active SFCL prototype.

4.1. Commissioning Test. Figure 6 shows the demonstration of the experimental circuit for testing the active SFCL prototype, and the commissioning works are carried out to evaluate the dynamic response behaviors of the prototype. The source voltage is set to 21 V, and the voltage over the supercapacitor units is charged to 40 V. Taking A phase as an example, Figures 7–9 show the active SFCL prototype's performance behaviors which include (1) starting and ending characteristics, (2) phase-regulating characteristic, and (3) transient characteristics under different capacitor voltages.

From Figure 7(a), the active SFCL prototype can start and put into action once the control of the converter is activated. Note that the test of the starting characteristic is to aim at mode 3 of the active SFCL, since mode 1 is triggered automatically. The active SFCL prototype can be launched quickly and effectively, and the changes of u_{1a}, i_{2a}, and u_{2a} show the details. From Figure 7(b), the active SFCL prototype can switch to its original operation state and have little influence on the main system obediently and reliably. Thus, the end of the current-limiting mode is also highly controlled.

From Figure 8, the phase-regulating characteristic of the active SFCL prototype is verified. The phase angle of the winding voltage u_{1a} is controlled to be approximately the same as that of the source voltage u_{sa}, and the SFCL prototype can offer a potential voltage compensation effect. According to Figure 9, the influence of adjusting the voltage u_{dc} on the performance of the active SFCL prototype can be observed. For the voltage u_{dc} is, respectively, set as 40 V and 80 V, the effects of the active SFCL prototype on controlling the amplitude values of the primary voltage, secondary voltage, and secondary current are, respectively, tested. Along with

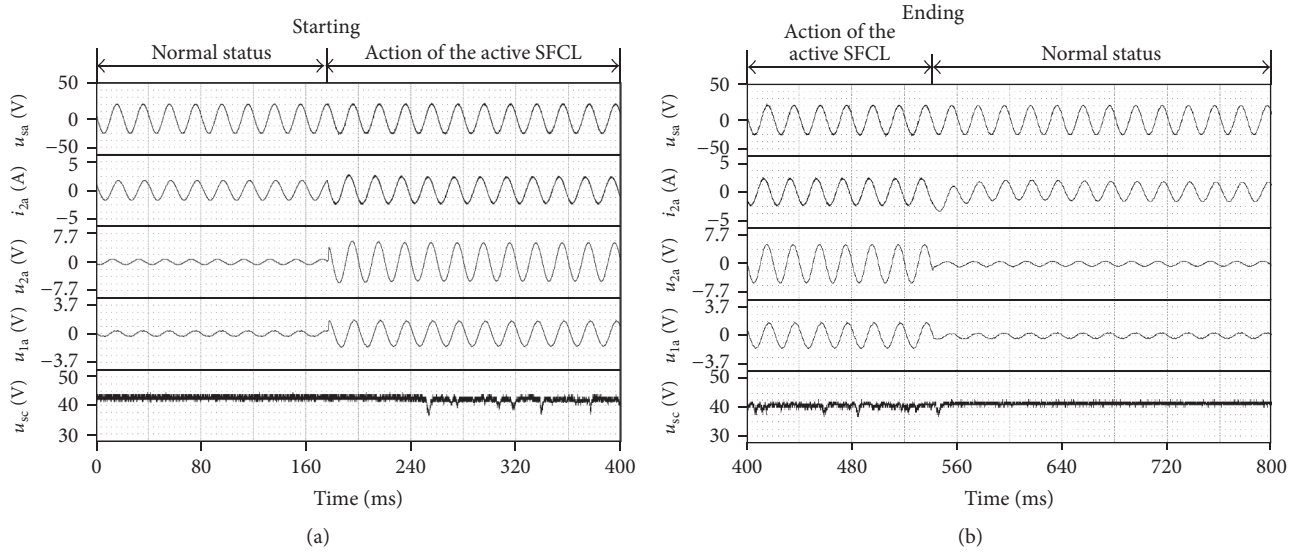

Figure 7: Performance of the active SFCL prototype under the commissioning test. (a) Starting characteristic and (b) ending characteristic.

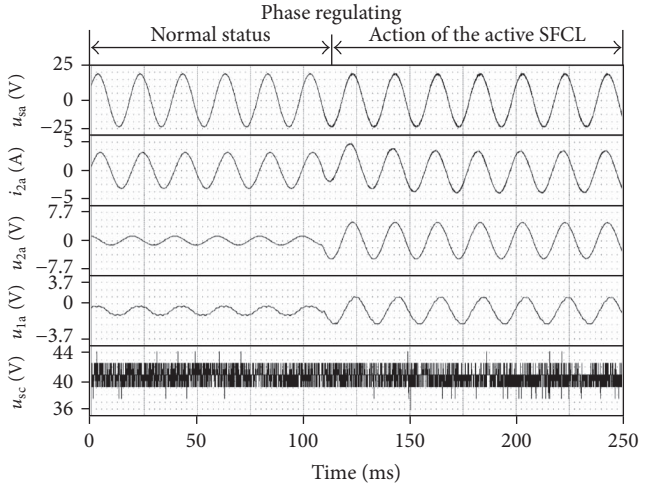

Figure 8: Phase-regulating characteristic of the active SFCL prototype under the commissioning test.

the increase of the DC voltage, the SFCL prototype will have a sufficient capacity margin to control u_{1a}, i_{2a}, and u_{2a}. In the current-limiting test, the capacitor voltage is enhanced further, and the SFCL prototype can obtain an enough capacity to handle the fault issues caused in a 132 V test system.

4.2. Current-Limiting Test. The circuit diagram of the current-limiting test is the same as that of the commissioning test. The source voltage is adjusted as 132 V; $Z_1 = 3\,\Omega$ and $Z_2 = 7\,\Omega$ are selected; the voltage over the supercapacitor units is charged to 400 V. In normal condition, the line current is about 13.2 A, and when Z_2 is short-circuited by the fault switch, the fault current will increase to 44 A without SFCL.

Figure 10 shows the performance of the SFCL prototype under the current-limiting mode 1. It is found that the active SFCL can automatically suppress the fault current to 33 A, and the expected current-limiting ratio is about 25%. Figure 11 shows the operation characteristics of the active SFCL prototype under the switching from mode 1 to mode 3. As a result, the fault current can be further reduced to 27 A, and the expected current-limiting ratio is about 38.6%. For this case, the SFCL prototype will offer a compensation voltage with the amplitude value of 49 V in series with the main circuit, and a slight fluctuation can be found in the DC voltage u_{dc}. In regard to the limitations of this SFCL prototype, its performance will be mainly constrained by the primary inductance of the air-core superconducting transformer and the capacity of the PWM converter. For the former, it is determined by the superconducting transformer's parameter design, and for the latter, it is determined by the energy storage unit in the PWM converter. On the whole, the stabilization of the DC voltage can be ensured, and the combination of the air-core superconducting transformer and the converter can well deal with the demonstrated short-circuit fault.

The active SFCL's contributions in alleviating the fault current, supporting the compensation voltage, and offering the high controllability can be confirmed by the experimental tests, and this kind of SFCL may have a wide application prospect in the power industry. Taking a 10 kW class PMSG-based wind turbine system as an example, the active SFCL's potential effects on enhancing the system performance and assisting the LVRT operation are studied in the following section.

5. Expanding Application of the Active SFCL in a PMSG-Based Wind Turbine System

As shown in Figure 12, it indicates the schematic diagram of a PMSG-based wind turbine system integrated with the active

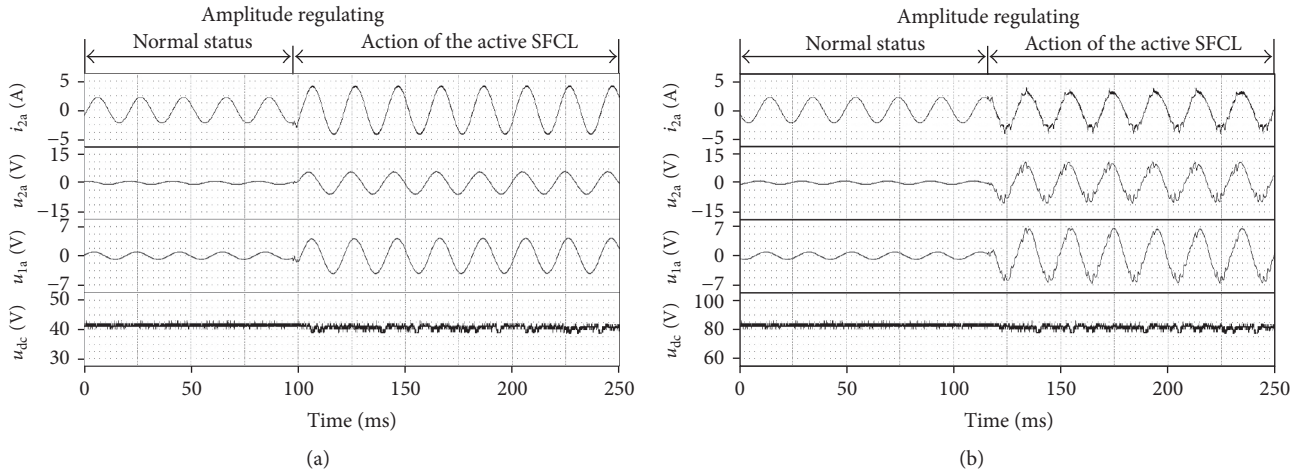

Figure 9: Influence of adjusting the capacitor voltage on the active SFCL prototype under the commissioning test. (a) $u_{dc} = 40$ V and (b) $u_{dc} = 80$ V.

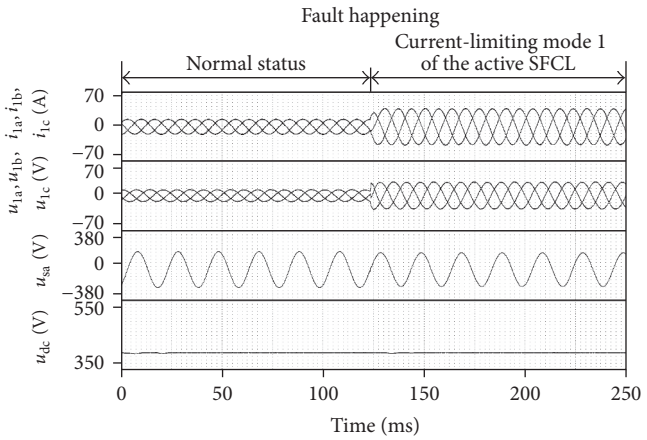

Figure 10: Performance of the active SFCL prototype corresponding to mode 1 under the current-limiting test.

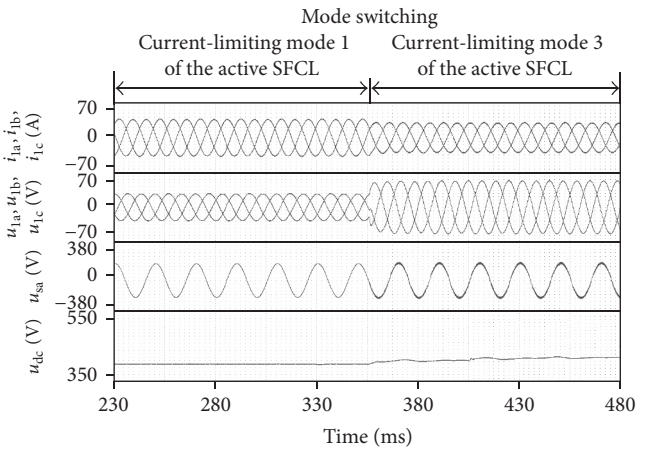

Figure 11: Performance of the active SFCL prototype corresponding to mode 3 under the current-limiting test.

SFCL. From this figure, the wind generation system will be coupled to the main network through the active SFCL and the step-up transformer. For the active SFCL's installation site, it is actually the point of common coupling (PCC) between the wind generation system and the set-up transformer.

When the wind generation system is under normal condition, it will send the wind energy to the main network as much as possible. The generator side converter (GSC) will use a traditional maximum power point tracking (MPPT) control, and the line-side converter (LSC) is to control the DC-link voltage. Due to the achievement of power balance, the following equations are derived:

$$P_{gen} = P_t - J_{eq}\omega_m \frac{d\omega_m}{dt} - P_{g\text{-loss}}$$
$$P_{cap} = C_{dc1}\frac{dV_{dc1}}{dt}V_{dc1} = P_{gen} - P_{grid}, \quad (2)$$

where P_{gen} is the generator power; P_t is the turbine power; $P_{g\text{-loss}}$ is the generator loss; P_{cap} is the capacitor power; P_{grid} is the grid-side power; C_{dc1} is the capacitor; V_{dc1} is the DC-link voltage over the capacitance.

Once the short-circuit fault occurs on the main network, the drop of the PCC voltage is inevitably caused, and also the original power balance will be damaged. The MPPT control will proceed to transmit the maximum power output of the wind turbine to the DC-link, but the grid-side power will decrease from P_{grid} to $P_{grid\text{-}f}$. Thus, the imbalance between P_{gen} and $P_{grid\text{-}f}$ will charge the DC-link capacitance, and the DC-link voltage under the fault is expressed as

$$V_{dc1\text{-}f} = \sqrt{\frac{2\left(P_{gen} - P_{grid\text{-}f}\right)\Delta t}{C_{dc1}} + V_{dc1}^2}, \quad (3)$$

where V_{dc1} and $V_{dc1\text{-}f}$ denote the DC-link capacitance voltage before and after the fault and Δt is the duration of the fault.

For the active SFCL is installed at the wind generation system, introducing the impedance Z_{SFCL} can help to consume the surplus power, suppress the grid-side currents,

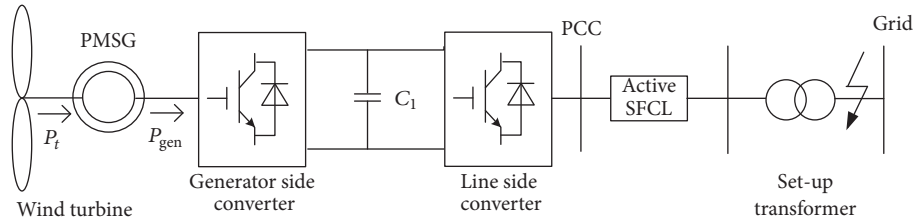

Figure 12: Schematic diagram of a PMSG-based wind turbine system integrated with the active SFCL.

Table 4: Specifications of the PMSG wind turbine system.

PMSG wind turbine system	
Rated active power	10 kW
DC-link voltage/capacitor	500 V/100 uF
Voltage source inverter's AC side	260 V/50 Hz
Set-up transformer	260 V/10.5 kV, 20 kVA

and compensate the voltage sags. To obtain the quantitative results, a simulation model corresponding to Figure 12 is built in MATLAB/Simulink, and Table 4 shows the main parameters of the 10 kW PMSG-based wind turbine system. As the power capacity of the wind turbine is equal to that of the AC/DC converter for the SFCL prototype, the prototype parameters as shown in Tables 1–3 will be also used for the simulation modeling of the active SFCL.

During the transient simulations, both of symmetrical and asymmetrical faults are taken into account. Concerning the specific LVRT code which the wind generation system should follow, the Denmark code is selectively used [31]. In the case where the main voltage drops to 20% of the nominal level, the wind generation system should remain in the grid-connected state for a duration of 150 ms.

5.1. Symmetrical Fault. The simulation conditions of a symmetrical fault are defined as follows: a three-phase line-to-ground fault is supposed to happen on the main network at $t = 2$ s; the fault resistance is $R_g = 1\,\Omega$ [32, 33]; the fault duration is 170 ms. Figure 13 shows the three-phase voltage characteristics of the wind generation system. During the process of the fault feeding, the wind generation system's output voltage coupled to the AC side will decrease from 200 V to 36 V (peak value). In other words, the main voltage will drop to 18% of the nominal level. The wind generation system cannot endure this severe voltage drop, and it will be enforcedly separated from the main network.

Regarding the control of the active SFCL, its current-limiting mode 1 and mode 3 are both simulated. Figure 14 shows the behaviors of the active SFCL in limiting the PCC fault current under the symmetrical fault. Mode 3 of the active SFCL can suppress the fault current to 33 A; compared to that, the fault current will increase to 140 A without SFCL.

Figure 15 shows the curves of the PCC power under different conditions. In the case without SFCL, the grid-side

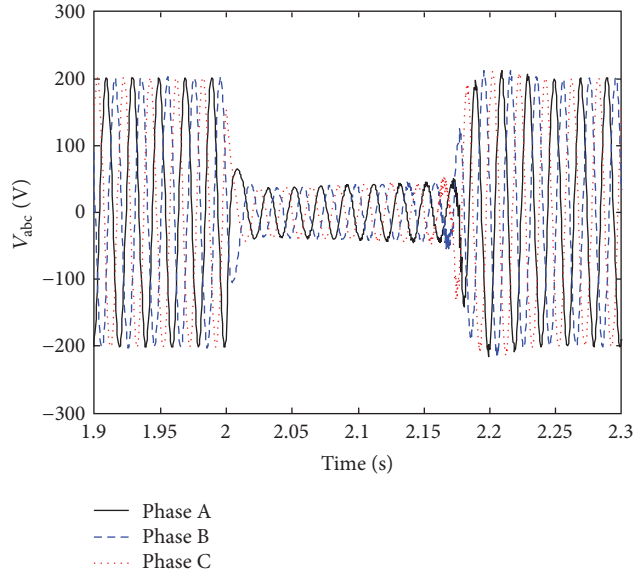

Figure 13: Three-phase voltage characteristics of the wind generation system under the symmetrical fault.

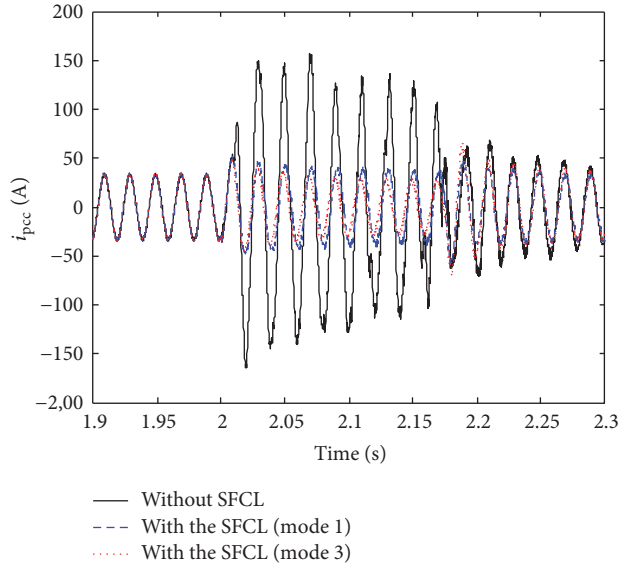

Figure 14: Behaviors of the active SFCL in limiting the PCC fault current under the symmetrical fault (A-phase).

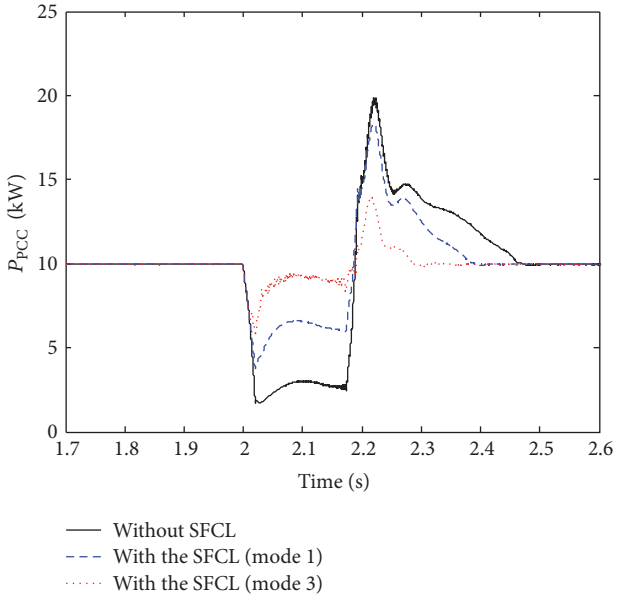

Figure 15: Effects of the active SFCL on the PCC power under the symmetrical fault.

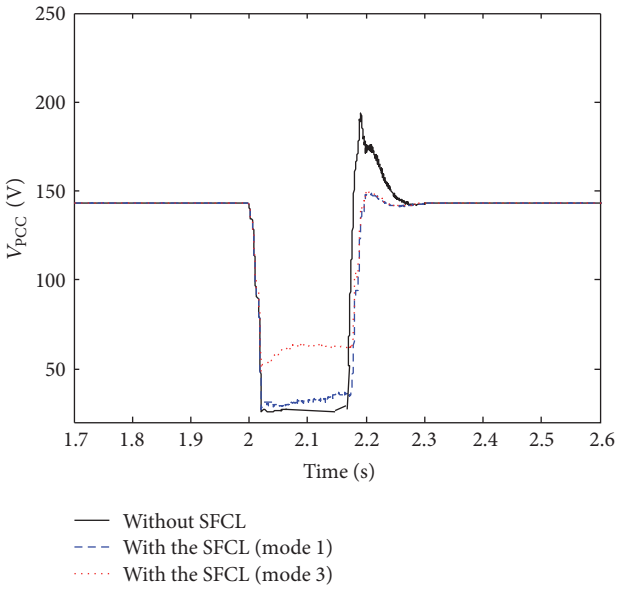

Figure 16: Effects of the active SFCL on the PCC voltage under the symmetrical fault.

power to the PCC decreases from 10 kW to 3 kW, and it will cause a serious power imbalance since the output power of the wind turbine is constant. For mode 1 and mode 3 of the active SFCL are, respectively, adopted, the PCC power can be maintained at 6 kW and 9 kW, respectively. In a sense, the improvement of the PCC power is able to enhance the utilization efficiency of the wind generation system.

Figure 16 shows the effects of the active SFCL on the PCC voltage under the symmetrical fault, and the vertical axis of this figure is to describe the root mean square (RMS) value of the A-phase PCC voltage. For mode 3 of the active

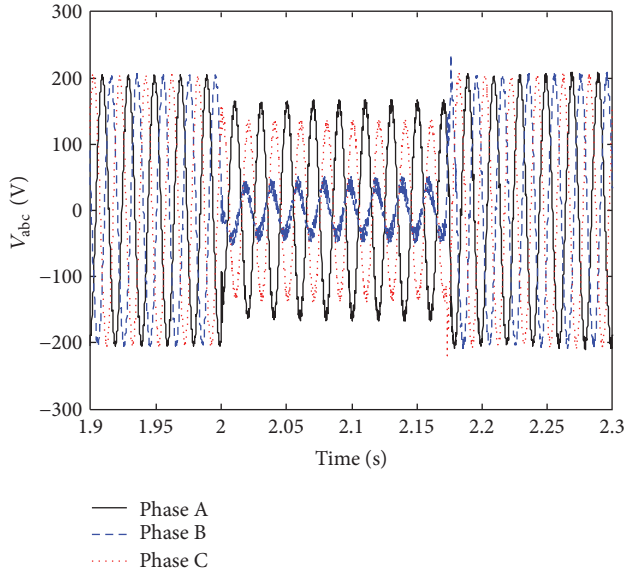

Figure 17: Three-phase voltage characteristics of the wind generation system under the asymmetrical fault.

SFCL is activated, the PCC voltage can be improved to 47% of the nominal level, and the wind generation system can successfully achieve the LVRT operation.

5.2. Asymmetrical Fault. To investigate the active SFCL's impacts on the wind generation system under the asymmetrical fault, a double-phase (A phase and B phase) line-to-ground fault is supposed to happen on the main network at $t = 2$ s. It should be pointed out that the possible asymmetrical fault scenarios include single-phase line-to-ground fault, double-phase line-to-line fault, and double-phase line-to-ground fault. Considering the severity level of a fault, the double-phase line-to-ground fault is the most serious among these asymmetrical fault scenarios. As a result, it is chosen to assess the performance behaviors of the active SFCL in the PMSG-based wind turbine system under an asymmetrical fault. The simulation parameters of the fault resistance and the fault duration are the same as the above symmetrical fault.

Figure 17 shows the wind generation system's three-phase voltage characteristics under this fault scenario. The simulation results reflect that the three-phase unbalance will be very obvious, and the B phase voltage will have the lowest amplitude level. During the process of the fault feeding, the B phase voltage's peak value will decrease from 200 V to 40 V, and it will exactly drop to 20% of the nominal level. In respect to the A phase and C phase voltages, their rates of decline are about 17.5% and 32.6%, respectively.

Figure 18 shows the influence of the active SFCL on the PCC power under the asymmetrical fault. In the event without SFCL, the PCC power will reduce from 10 kW to 7 kW, and mode 3 of the active SFCL can maintain the power balance and mitigate the power fluctuation as much as possible.

Figure 19 indicates the influence of the active SFCL on the PCC voltage under the asymmetrical fault. For mode 3

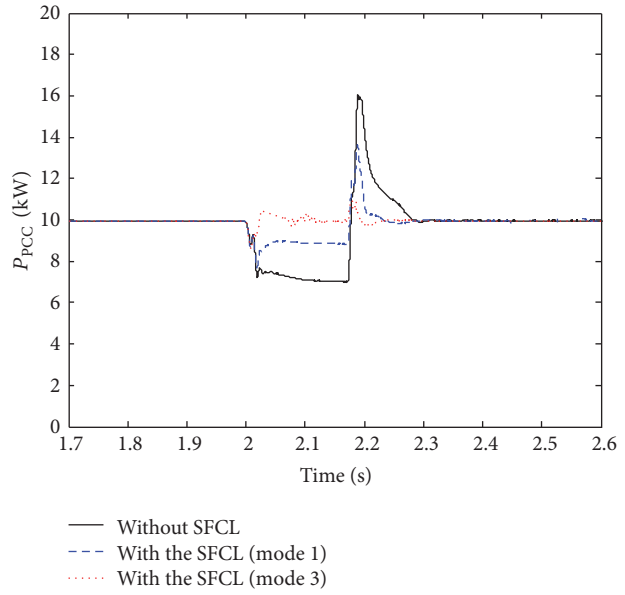

Figure 18: Influence of the active SFCL on the PCC power under the asymmetrical fault.

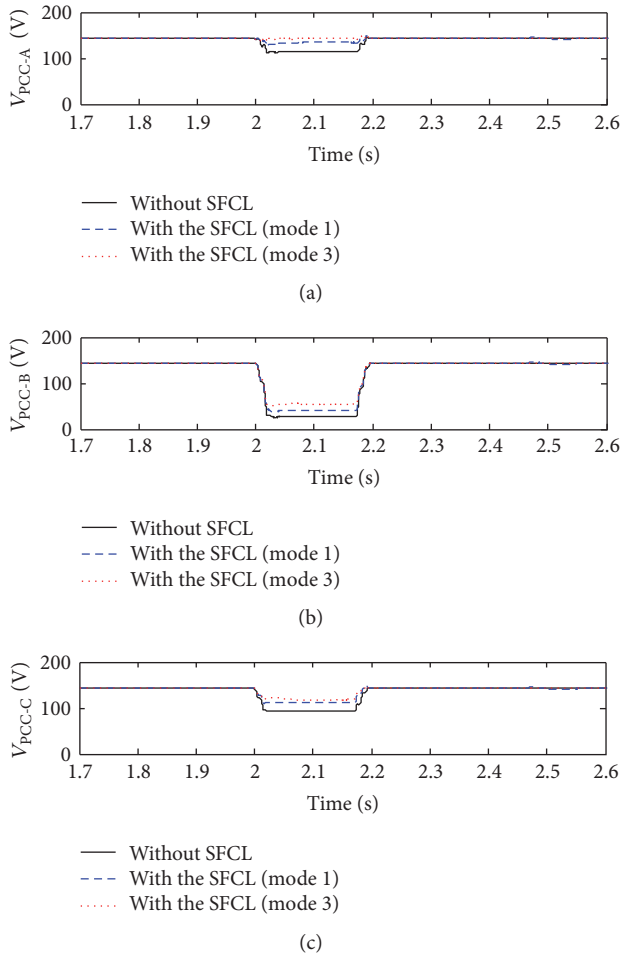

Figure 19: Influence of the active SFCL on the PCC voltage under the asymmetrical fault.

of the active SFCL is applied, the B phase PCC voltage can be enhanced to 41% of the nominal level, and some minor effects on compensating A phase and C phase PCC voltages can be also obtained.

From the demonstrated figures, the function of the active SFCL to alleviate the three-phase imbalance can be enhanced. One possible solution is to explore an optimal control of the positive, negative, and zero sequence components of the injected currents, so as to make the active SFCL handle the asymmetrical fault more efficiently. The performance optimization study will be done in the succeeding works.

6. Conclusions

Concerning the development of a voltage compensation type active SFCL and its application for transient performance enhancement of a PMSG-based wind turbine system, related theoretical analyses, experimental tests, and simulation studies are conducted in this paper. The following conclusions can be obtained:

(1) According to the commissioning test and the current-limiting test, the active SFCL prototype can automatically suppress the fault current and offer a highly controllable compensation voltage in series with the main network. In consideration of the transfer between different operation modes, the active SFCL prototype's current-limiting and voltage-compensating performance can be enhanced further.

(2) Based on the application of the active SFCL in a PMSG-based wind turbine system, transient performance enhancement can be found from multiple aspects. Using the active SFCL can help to maintain the PCC power balance, mitigate the PCC voltage-current fluctuation, and improve the wind energy efficiency. The active SFCL can be regarded as a feasible solution to assist the wind generation system to achieve the LVRT operation.

In the near future, some follow-up works will be undertaken, such as the robustness improvement of the active SFCL to deal with the asymmetrical fault and the experimental tests of the active SFCL in a real renewable energy system. In addition, for the possible interaction between the voltage compensation type active SFCL and power system during its actual application, there are many technical issues needed to be handled, such as optimized installation sites, coordination with circuit breakers, and cooperation among multiple SFCLs. These tasks will be carried out in our follow-up plans, and the research results will be reported in later articles.

Conflicts of Interest

The authors declare that there are no conflicts of interest regarding the publication of this paper.

Acknowledgments

This work was supported by the National Natural Science Foundation of China (51507117).

References

[1] Y. Wang and Y. Zheng, "Review of research and measurement for application properties of HTS tapes," *Science China Technological Sciences*, vol. 57, no. 8, pp. 1568–1577, 2014.

[2] Y. Wang, W. Zhou, and J. Dai, "An applicable calorimetric method for measuring AC losses of 2G HTS wire using optical FBG," *Science China Technological Sciences*, vol. 58, no. 3, pp. 545–550, 2015.

[3] X. Zhang, H. S. Ruiz, J. Geng, and T. A. Coombs, "Optimal location and minimum number of superconducting fault current limiters for the protection of power grids," *International Journal of Electrical Power & Energy Systems*, vol. 87, pp. 136–143, 2017.

[4] S. Alaraifi and M. S. El Moursi, "Design considerations of superconducting fault current limiters for power system stability enhancement," *IET Generation, Transmission & Distribution*, vol. 11, no. 9, pp. 2155–2163, 2017.

[5] J. Sun, H. Ohara, and S. Yamaguchi, "Experimental Study on Ferromagnetic Shunt Effects on the Critical Current of BSCCO Tape in Stacked Conductors," *Advances in Condensed Matter Physics*, vol. 2017, pp. 1–7, 2017.

[6] L. Chen, H. Chen, J. Yang, Z. Shu, H. He, and X. Shu, "Conceptual design of a high-speed electromagnetic switch for a modifed flux-coupling-type SFCL and its application in renewable energy system," *SpringerPlus*, vol. 5, pp. 771–785, 2016.

[7] F. Liang, W. Yuan, C. A. Baldan, M. Zhang, and J. S. Lamas, "Modeling and experiment of the current limiting performance of a resistive superconducting fault current limiter in the experimental system," *Journal of Superconductivity and Novel Magnetism*, vol. 28, no. 9, pp. 2669–2681, 2015.

[8] L. Chen, X. Tu, H. Chen et al., "Technical evaluation of superconducting fault current limiters used in a micro-grid by considering the fault characteristics of distributed generation, energy storage and power loads," *Energies*, vol. 9, pp. 769–789, 2016.

[9] J. Zhu, Y. Li, and X. Duan, "Application of SFCLs to inhibit commutation failure in HVdc systems: position comparison and resistance recommendation," *Canadian Journal of Electrical and Computer Engineering*, vol. 40, no. 1, pp. 31–40, 2017.

[10] W. Sanusi, M. Al Hosani, and M. S. El Moursi, "A novel DC fault ride-through scheme for MTDC networks connecting large-scale wind parks," *IEEE Transactions on Sustainable Energy*, vol. 8, p. 1086, 2017.

[11] W. Guo, L. Xiao, and S. Dai, "Enhancing low-voltage ride-through capability and smoothing output power of DFIG with a superconducting fault-current limiter–magnetic energy storage system," *IEEE Transactions on Energy Conversion*, vol. 27, no. 2, pp. 277–295, 2012.

[12] M. E. Elshiekh, D.-E. A. Mansour, and A. M. Azmy, "Improving fault ride-through capability of DFIG-based wind turbine using superconducting fault current limiter," *IEEE Transactions on Applied Superconductivity*, vol. 23, no. 3, Article ID 5601204, 2013.

[13] L. Chen, C. Deng, F. Zheng, S. Li, Y. Liu, and Y. Liao, "Fault ride-through capability enhancement of DFIG-based wind turbine with a flux-coupling-type SFCL employed at different locations," *IEEE Transactions on Applied Superconductivity*, vol. 25, no. 3, Article ID 5201505, 2015.

[14] E. A. Mohamed, Y. Qudaih, Y. Mitani, and M. Ebeed, "Study the different effects of SFCL and outer crowbar on fault ride-through capability enhancement of wind farms," *Energy Procedia*, vol. 100, pp. 127–136, 2016.

[15] M. M. Hossain and M. H. Ali, "Transient stability improvement of doubly fed induction generator based variable speed wind generator using DC resistive fault current limiter," *IET Renewable Power Generation*, vol. 10, no. 2, pp. 150–157, 2016.

[16] S. B. Naderi, M. Negnevitsky, A. Jalilian, M. T. Hagh, and K. M. Muttaqi, "Low voltage ride-through enhancement of DFIG-based wind turbine using DC link switchable resistive type fault current limiter," *International Journal of Electrical Power & Energy Systems*, vol. 86, pp. 104–119, 2017.

[17] U. A. Khan, W. J. Shin, J. K. Seong, S. H. Oh, S. H. Lee, and B. W. Lee, "Feasibility analysis of the application and positioning of DC HTS FCL in a DC microgrid through modeling and simulation using Simulink and SimPowerSystem," *Physica C: Superconductivity and Its Applications*, vol. 471, no. 21, pp. 1322–1326, 2011.

[18] J.-S. Hwang, U. A. Khan, W.-J. Shin et al., "Validity analysis on the positioning of superconducting fault current limiter in neighboring AC and DC microgrid," *IEEE Transactions on Applied Superconductivity*, vol. 23, no. 3, Article ID 5600204, 2013.

[19] S. R. Khuntia and S. R. Samantaray, "Analysis of resistive SFCL in a test-bed microgrid," *Ain Shams Engineering Journal*, vol. 6, no. 3, pp. 883–892, 2015.

[20] L. Chen, H. He, L. Zhu et al., "Coordinated control of SFCL and SMES for transient performance improvement of microgrid with multiple DG units," *Canadian Journal of Electrical and Computer Engineering*, vol. 39, no. 2, pp. 158–167, 2016.

[21] B. Singh, V. Mukherjee, and P. Tiwari, "A survey on impact assessment of DG and FACTS controllers in power systems," *Renewable and Sustainable Energy Reviews*, vol. 42, pp. 846–882, 2015.

[22] B. Zhao, Y. Yang, X. Zhang et al., "Implementation of a dual-microgrid system with flexible configurations and hierarchical control in China," *Renewable and Sustainable Energy Reviews*, vol. 65, pp. 113–123, 2016.

[23] L. Chen, Y. Tang, J. Shi, and Z. Sun, "Simulations and experimental analyses of the active superconducting fault current limiter," *Physica C: Superconductivity*, vol. 459, no. 1, pp. 27–32, 2007.

[24] L. Chen, Y. J. Tang, J. Shi et al., "Influence of a voltage compensation type active superconducting fault current limiter on the transient stability of power system," *Physica C: Superconductivity*, vol. 469, pp. 1760–1764, 2009.

[25] L. Chen, Y. J. Tang, J. Shi, Z. Li, L. Ren, and S. J. Cheng, "Control strategy for three-phase four-wire PWM converter of integrated voltage compensation type active SFCL," *Physica C: Superconductivity*, vol. 470, no. 3, pp. 231–235, 2010.

[26] L. Chen, Y. J. Tang, J. Shi et al., "Effects of a voltage compensation type active superconducting fault current limiter on distance relay protection," *Physica C: Superconductivity and Its Applications*, vol. 470, no. 20, pp. 1662–1665, 2010.

[27] L. Chen, C. Deng, F. Guo, Y. Tang, J. Shi, and L. Ren, "Reducing the fault current and overvoltage in a distribution system with distributed generation units through an active type SFCL," *IEEE Transactions on Applied Superconductivity*, vol. 24, no. 3, Article ID 5600305, 2014.

[28] L. Chen, F. Zheng, C. Deng, Z. Li, and F. Guo, "Fault ride-through capability improvement of DFIG-based wind turbine by employing a voltage-compensation-type active SFCL," *Canadian Journal of Electrical and Computer Engineering*, vol. 38, no. 2, pp. 132–142, 2015.

[29] M. Song, Y. Tang, Y. Zhou, L. Ren, L. Chen, and S. Cheng, "Electromagnetic characteristics analysis of air-core transformer used in voltage compensation type active SFCL," *IEEE Transactions on Applied Superconductivity*, vol. 20, p. 1194, 2010.

[30] J. Wang, L. Zhou, J. Shi, and Y. Tang, "Experimental investigation of an active superconducting current controller," *IEEE Transactions on Applied Superconductivity*, vol. 21, no. 3, pp. 1258–1262, 2011.

[31] Y. Yang, F. Blaabjerg, and Z. Zou, "Benchmarking of Grid Fault Modes in Single-Phase Grid-Connected Photovoltaic Systems," *IEEE Transactions on Industry Applications*, vol. 49, no. 5, pp. 2167–2176, 2013.

[32] S. A. Gopalan, V. Sreeram, and H. H. C. Iu, "A review of coordination strategies and protection schemes for microgrids," *Renewable and Sustainable Energy Reviews*, vol. 32, pp. 222–228, 2014.

[33] R. Mohanty, U. S. M. Balaji, and A. K. Pradhan, "An accurate noniterative fault-location technique for low-voltage DC microgrid," *IEEE Transactions on Power Delivery*, vol. 31, no. 2, pp. 475–481, 2016.